First-principles insight into the degeneracy of ground-state LiBH_{4} structures

Yongsheng Zhang, Yongli Wang, Kyle Michel, and C. Wolverton

Phys. Rev. B **86**, 094111 — Published 19 September 2012

DOI: 10.1103/PhysRevB.86.094111

First-principles insight into the degeneracy of ground state $LiBH_4$ structures

Yongsheng Zhang, Yongli Wang, Kyle Michel, and C. Wolverton
Department of Materials Science & Engineering,
Northwestern University, Evanston, Illinois 60208, USA

(Dated: September 10, 2012)

Recently, a number of ground-state structures of $LiBH_4$ have been proposed, both from experimental and computational works. The results show controversy between computational and experimental ground state crystal structures of $LiBH_4$. In order to determine which is truly the lowest in energy, we study $LiBH_4$ in a variety of crystal structures using density-functional theory (DFT) calculations of the free energy (T=0 K total energy plus vibrational thermodynamics), employing a variety of DFT methods and exchange-correlation functionals. Our calculations show that the experimentally observed structures are lowest in energy in DFT. However, multiple $LiBH_4$ structures are degenerate with the experimental ground state crystal structure and there exists a relatively flat potential energy landscape between them. These degenerate structures include the recently theoretically predicted $LiBH_4$ structure [Phys. Rev. Lett. **104**, 215501 (2010)], which the authors claimed to be 9.66 kJ/(mol $LiBH_4$) (or $\sim$100 meV/fu) lower in energy than the experimentally XRD determined $LiBH_4$ structure [J. Alloys Compd. **346**, 200 (2002)]. Our calculations do not support these previous claims, and hence resolve this discrepancy between DFT and experiment.

PACS numbers: 61.50.Ah, 61.66.Fn, 63.20.-e, 65.40.-b

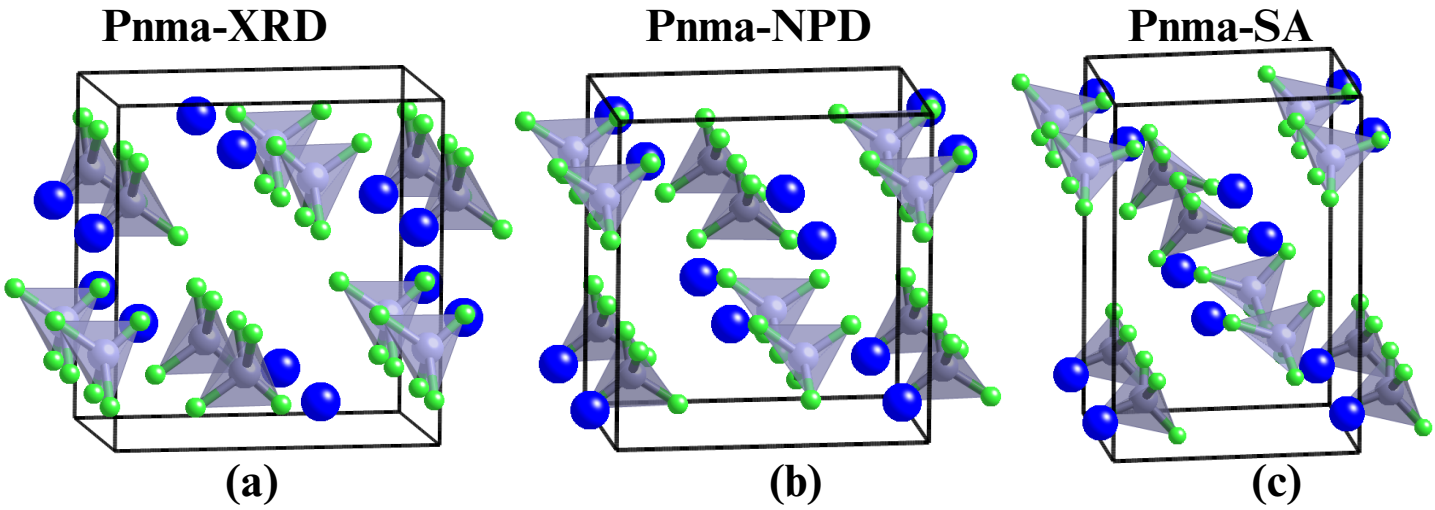

FIG. 1. (Color online) Crystal structures of the three $LiBH_4$ structures [(a): Pnma-XRD[8], (b): Pnma-NPD[9] and (c): Pnma-SA[10]]. They all have the same Pnma space group, but different lattice constants (Table I). Big blue spheres, grey spheres and small green spheres represent Li, B and H atoms, repressively. Light grey polydehra represent [BH_4] units.

Metal borohydrides[1–3] [$M(BH_4)_n$, where M is an alkali or alkaline earth metal] have received considerable attention as hydrogen storage materials due to their high gravimetric capacities of hydrogen. In particular, $LiBH_4$[4–7] contains 18.3 wt.% H_2, which, if fully released, would be well above the system target for passenger vehicles.[2,3] The $LiBH_4$ crystal structure has been experimentally investigated using X-ray diffraction (XRD) at 293 K by Soulié *et al.*[8] and at 90 K by Filinchuk *et al.*[5], and using neutron powder diffraction (NPD) at 3.5 K by Hartman *et al.*[9]. In all of these experimental studies[5,8,9], the authors suggest that the $LiBH_4$ structure is in the Pnma space group over a wide range of temperatures (3.5, 90 and 293 K). The $LiBH_4$ crystal structures (lattice constants and atomic positions) proposed in the Hartman *et al.*[9] and Filinchuk *et al.*[5] works are nearly the same (both relax to the same structure in our DFT calculations). The structure proposed by Soulié XRD[8] is slightly different than those other two, mainly is the positions of the hydrogen atoms. [The experimental XRD and NPD determined $LiBH_4$ Pnma structures are denoted as Pnma-XRD (Fig. 1-a) and Pnma-NPD (Fig. 1-b) in the paper, respectively.]

In recent work[10], Tekin *et al.* used a simulated annealing (SA) method to predict low-energy structures of $LiBH_4$ using the pseudopotential DFT code CASTEP. They surprisingly report six structures that are lower in energy than the $LiBH_4$ structure determined by Soulié using XRD (Pnma-XRD, Fig. 1-a). In particular, Tekin *et al.*[10] found that their theoretically predicted $LiBH_4$ ground state structure also has the Pnma space group (we denote the structure as Pnma-SA, Fig. 1-c), and these authors found that their predicted Pnma-SA structure is 9.66 kJ/(mol $LiBH_4$) (or ∼100 meV/fu) lower in energy than the Soulié Pnma-XRD $LiBH_4$ structure.

Reliable low-T or ground-state structures play a vital role in understanding the properties of complex metal hydrides, such as decomposition pathways; a 10 kJ/(mol $LiBH_4$) energy difference in the $LiBH_4$ compound can change the calculated H_2 released temperature by ∼100 K in the thermodynamic stable reaction[11] ($LiBH_4 \rightarrow \frac{1}{12}Li_2B_{12}H_{12} + \frac{5}{6}LiH + \frac{13}{12}H_2$). Therefore, it is important to understand if the lowest-energy structure of $LiBH_4$ predicted by Tekin *et al.* truly is ∼10 kJ/(mol $LiBH_4$) lower in energy than the observed structure. We also notice that Tekin *et al.*[10] omitted the experimental NPD determined $LiBH_4$ structure from Hartman (Pnma-NPD, Fig. 1-b), which we have included here. In this paper, we use density-functional theory (DFT) with various exchange-correlation functionals and potentials to probe these experimentally determined (Pnma-XRD and Pnma-NPD) and theoretically predicted (Pnma-SA) $LiBH_4$ crystal structures. From our DFT calculations with frozen phonon approximations, we show that the theoretically predicted Pnma-SA $LiBH_4$ structure (Fig. 1-c) *does not have a lower energy* than the experimentally observed Pnma-XRD structure (Fig. 1-a); instead these energies are degenerate, and a relatively flat potential energy landscape exists between them. Our calculations thus resolve the contradiction between experimentally reported and DFT predicted structures of $LiBH_4$.

We perform DFT calculations using the Vienna Ab Initio Simulation Package (VASP) code with the projector augmented wave (PAW) scheme[12]. We use the exchange-correlation functional (XC) from the generalized gradient approximation (GGA) proposed by Perdew, Burke and Ernzerhof (GGA-PBE)[13] as well as Perdew and Wang (GGA-PW91)[14]. The energy cutoff for the plane wave expansion is 875 eV. We treat $1s^2 2s^1$, and $2s^2 2p^1$ as valence electrons in Li and B atoms, respectively. Additionally, we perform calculations with ultra-soft pseudopotentials (US) and GGA-PW91 in VASP, which we compare to the previous US results on $LiBH_4$[7,10]. The Brillouin zones are sampled by

TABLE I. Lattice constants and selected interatomic distances of experimental XRD determined (Pnma-XRD)[8], NPD determined (Pnma-NPD)[9] and theoretically predicted (Pnma-SA)[10] $LiBH_4$ structures. The corresponding values of our DFT relaxations using different XC (PBE and PW91) and potentials (PAW and US) are also presented. (units: Å)

Lattice constants	Pnma-XRD	Pnma-NPD	Pnma-SA
Previous work	7.18, 4.44, 6.80 (exp.[8])	7.12, 4.41, 6.67 (exp.[9])	8.48, 4.35, 5.75 (the.[10])
PAW-PBE (present work)	7.28, 4.38, 6.60	7.38, 4.38, 6.55	8.62, 4.36, 5.69
PAW-PW91 (present work)	7.32, 4.37, 6.59	7.33, 4.38, 6.58	8.62, 4.36, 5.72
US-PW91 (present work)	7.32, 4.37, 6.54	7.31, 4.37, 6.55	8.54, 4.35, 5.74

Interatomic distances	Pnma-XRD	Pnma-NPD	Pnma-SA
Li-4B (previous work)	2.47−2.54 (exp.[8])	2.37−2.54 (exp.[9])	2.41−2.55 (the.[10])
Li-4B (present work: PAW-PBE)	2.34−2.53	2.33−2.54	2.43−2.56
B-4H (previous work)	1.03−1.28 (exp.[8])	1.21 (exp.[9])	1.22 (the.[10])
B-4H (present work: PAW-PBE)	1.22	1.22	1.23

TABLE II. Static energy differences (without phonon contributions) of the three $LiBH_4$ structures (Pnma-XRD[8], Pnma-NPD[9] and Pnma-SA[10]) calculated by DFT using different XC (PBE and PW91) and different potentials (PAW, US and FLAPW). The value is the energy difference relative to the lowest DFT energy in each row. (units: meV/fu)

	Pnma-XRD	Pnma-NPD	Pnma-SA
PAW-PBE (unrelaxed)	896	6	0
PAW-PBE (fully relaxed)	0	0	2
PAW-PW91 (fully relaxed)	0	0	1
US-PW91 (fully relaxed)	0.2	0.2	0
FLAPW-PBE(unrelaxed)	903	6	0
FLAPW-PBE(PAW-PBE str.)	1	0	2

Monkhorst-Pack[16] k-point meshes chosen to give a roughly constant density of k-points ($30/\text{Å}^{-3}$) for all compounds. Atomic positions and unit cell parameters are completely relaxed using different XC and potentials in VASP (PAW-GGA-PBE, PAW-GGA-PW91 and US-GGA-PW91) until all forces and components of the stress tensor are below 0.01 eV/Å and 0.2 kbar, respectively. Phonons are calculated using the supercell force constant method (as implemented in the program described in Ref. 17) within the PAW-GGA-PBE scheme, and the vibrational entropies and enthalpies are obtained by integration over the calculated phonon density of states.

In order to test the accuracy of VASP-PAW calculations, we further use the PBE functional in the WIEN2k code[15], which implements the all-electron full-potential linearized augmented plane wave (FLAPW) method, to obtain the total energies of the $LiBH_4$ compounds. In the FLAPW calculations, Muffin tin spheres for Li, B and H are $R_{\text{MT}}^{\text{Li}} = 2.3\,\text{bohr}$, $R_{\text{MT}}^{\text{B}} = 1.4\,\text{bohr}$, and $R_{\text{MT}}^{\text{H}} = 0.5\,\text{bohr}$ respectively; the wave function expansion inside the muffin tin spheres is truncated at $l_{\text{max}}^{\text{wf}} = 12$, and the potential expansion at $l_{\text{max}}^{\text{pot}} = 6$. The energy cutoff for the plane wave representation in the interstitial region between the muffin tin spheres is $E_{\text{max}}^{\text{wf}} = 20\,\text{Ry}$ for the wave functions and $E_{\text{max}}^{\text{pot}} = 196\,\text{Ry}$ for the potential. Monkhorst-Pack grids used for the Brillouin zone integrations are the same as those used during VASP calculations.

In Table I, we show the lattice constants and selected interatomic distances of XRD determined (Pnma-XRD)[8], NPD determined (Pnma-NPD)[9] and theoretically predicted (Pnma-SA)[10] $LiBH_4$ structures. There are significant differences in the Pnma-NPD and -SA structures, especially in the lengths of the $\vec{a}$ and $\vec{c}$ basis vectors. Each structure is then fully relaxed using DFT (VASP) calculations. As shown in Table I, the resulting lattice constants are similar in calculations using different exchange-correlations (PBE and PW91) or potentials (PAW and US). The largest deviation in lattice constants between our results and those in the Refs. 8–10 is ∼0.2 Å. For the XRD determined $LiBH_4$ structure (Pnma-XRD), our relaxed lattice constants agree well with previous pseudopotential calculations (a=7.34 Å, b=4.40 Å, c=6.59 Å) from Miwa *et al.*[7] and (a=7.25 Å, b=4.37 Å, c=6.56 Å) from Tekin *et al.*[10] For the interatomic distances such as Li-B and B-H (Table I), our DFT relaxed distances of Pnma-NPD and -SA $LiBH_4$ structures are similar to those in the Refs. 9 and 10, respectively. However, we find differences of 0.13 Å and 0.2 Å in the Li-B and B-H distances when comparing the experimental XRD determined structure (Pnma-XRD) with those

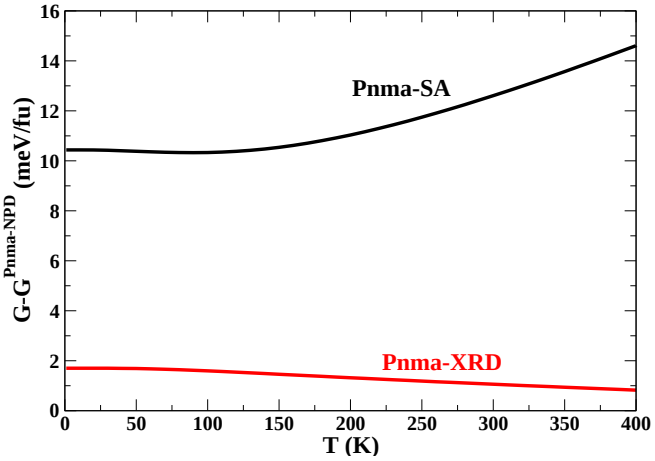

FIG. 2. (Color online) Gibbs free energy differences of $LiBH_4$ at different temperatures with respect to the free energies of the Pnma-NPD $LiBH_4$ structure. The black and red lines represent the relative Gibbs free energies of the Pnma-SA and -XRD $LiBH_4$ structures, respectively.

in the corresponding DFT relaxed structures (Table I); we note that our B-H bond lengths are consistent with those from previous US-PBE calculations[7] (B-H: 1.23∼1.25Å).

The energies obtained from our static energy calculations (PAW-PBE, without vibrational contributions) are shown in Table II. For the three $LiBH_4$ structures taken from Refs[8–10], without geometry relaxations, our PAW-PBE calculations show that the energy of the Pnma-XRD $LiBH_4$ structure is much higher than that of the other two $LiBH_4$ structures (Pnma-SA and -NPD), due to a short B-H bond in the Pnma-XRD structure: 1.03 Å (Table I). Additionally, the energy of the Pnma-NPD $LiBH_4$ structure (Pnma-NPD) is only 6 meV/fu higher than that of the theoretically predicted $LiBH_4$ structure (Pnma-SA). Following geometry relaxations (Table II) of the three $LiBH_4$ structures (Pnma-XRD, -NPD and -SA), we find that the resulting energies are degenerate within ∼2 meV/fu (the theoretically predicted Pnma-SA $LiBH_4$ structure is even 2 meV/fu higher in energy than both the XRD and NPD structures). Furthermore, this degeneracy persists even when different potentials and XC (PAW-PW91 and US-PW91) are used (Table II). To test the accuracy of VASP-PAW calculations, we further use FLAPW with the PBE functional to obtain the total energies of the three $LiBH_4$ compounds using unrelaxed and VASP-PAW-PBE relaxed structures. We find that the energy differences (Table II) between the three $LiBH_4$ structures are very similar using the two potentials (FLAPW and PAW), which indicates that the projector augmented wave (PAW) approximations can accurately reproduce the energetic trends of the all-electron and full-potential method (FLAPW), and gives us confidence that the VASP-PAW results are reliable. Using the static energies shown in Table II, we find that the experimental structures are indeed the ground state and that the structure obtained from simulated annealing method (SA) is actually higher in energy (not ∼100 meV/fu lower as reported in Ref. 10).

To further understand the vibrational contributions (zero-point energy and finite-temperature effects) on the structural stabilities, we next calculate the Gibbs free energies (Fig. 2) of the three (DFT-relaxed) $LiBH_4$ structures (Pnma-XRD, -NPD and -SA). From Fig. 2, the free energies of the experimentally determined $LiBH_4$ structures (Pnma-XRD and -NPD) are clearly degenerate. We find the theoretically predicted Pnma-SA $LiBH_4$ structure is ∼10 meV/fu higher in energy than the ground state experimental structures (Pnma-XRD and -NPD), strongly contradicting the results in Ref. 10, where this structure is predicted to be ∼100 meV/fu below the experimental XRD structure (Pnma-XRD). Therefore, our results show that the theoretically predicted $LiBH_4$ structure (Pnma-SA) is not a the lowest-energy DFT structure as described in Ref. 10. Moreover, we calculate the formation enthalpy of $LiBH_4$ with respect to Li(bcc), B(α) and H_2(gas) at T=0K with ZPE by the method described in Ref. 10, and we get -154.8, -155.2 and -154.0 kJ/(mol $LiBH_4$) for the Pnma-XRD, -NPD and -SA $LiBH_4$ compounds, respectively. These values strongly deviate from the formation enthalpies in Ref. 10 [-230.330 and -239.988 kJ/(mol $LiBH_4$)] for the Pnma-XRD and Pnma-SA $LiBH_4$ structures, but agree well with the formation enthalpy of the Pnma-XRD structure from Miwa *et al.*[7] DFT-US-PBE calculations [-160 kJ/(mol $LiBH_4$)]. Even though the source of such large formation enthalpy differences between our work and Ref. 10 is currently unknown, our DFT calculations provide reliable results: with different exchange-correlations (PBE and PW91) or different potentials (PAW, US and FLAPW), all yield the consistent geometry and energetic results (Table I and II), and our results on the Pnma-XRD $LiBH_4$ structure are in good agreement with Miwa *et al.*[7] DFT-US-PBE calculations of geometries (lattice constants and bond lengths) and energetics (the formation enthalpy).

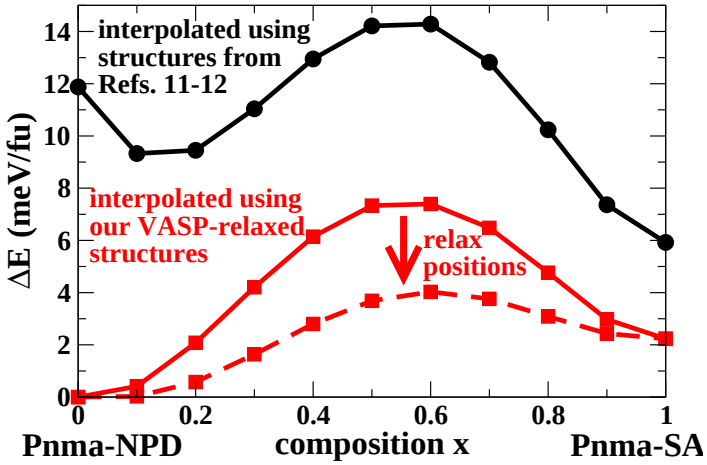

FIG. 3. (Color online) The $LiBH_4$ potential energy surface between the experimentally determined Pnma-NPD and theoretically predicted Pnma-SA $LiBH_4$ structures by interpolation (see text for detail). The black circles and the red squares (connected by a solid line) are the potential energy surface interpolated using the NPD and SA structures from Refs. 9 and 10, and from our VASP relaxations, respectively. The red squares (connected by a dashed line) represents the further atomic position relaxations of these interpolated structures. Note the very small energy scale of the figure, indicating a relatively flat potential landscape between the two structures.

Although the energies of the three $LiBH_4$ structures (Pnma-XRD, -NPD and -SA) are degenerate, it is interesting to notice that they have significantly different lattice constants (Table I), especially between the Pnma-NPD and -SA $LiBH_4$ structures (Table I), where $\vec{a}$ differs by ~ 1.3 Å and the volumes by $\sim$0.6 Å^3/fu. In order to better understand the energy landscape around these structures, we interpolate intermediate structures between the Pnma-NPD and -SA structures by changing the lattice constant and atomic positions at the same time [$a_i^{int} = x a_i^{SA} + (1-x) a_i^{NPD}; s_j^{int} = x s_j^{SA} + (1-x) s_j^{NPD}$, where a_i^{int}, a_i^{SA} a_i^{NPD}, s_j^{int}, s_j^{SA} and s_j^{NPD} are lattice constants (a_i=a, b, c) and the atomic positions (s_j, j=x, y, z) of the interpolated, Pnma-SA and Pnma-NPD $LiBH_4$ structures, respectively.]. The total energy of each interpolated structure is then calculated from PAW-PBE (Fig. 3). When we take the Pnma-SA and -NPD $LiBH_4$ structures directly from Refs. 9 and 10 (no geometry relaxations) to interpolate (the black circled line in Fig. 3), we see that the Pnma-NPD unrelaxed structure has a slightly higher energy ($\sim$6 meV/fu) than the theoretical Pnma-SA unrelaxed structure (Table II). As the interpolated structure moves towards the Pnma-SA structure, there is an initial decrease in the energy (since the reference states are not relaxed) followed by a relatively small barrier ($\sim$5 meV/fu). If the reference states (Pnma-SA and Pnma-NPD) are now fully relaxed, the interpolated path (the red squares + solid line in Fig. 3) between them is qualitatively different than the unrelaxed one (the black circled line in Fig. 3): the local minimum at x=0.1 disappears and the Pnma-SA structure is 2 meV/fu higher in energy than the NPD structure. Additionally, we find a 8 meV/fu barrier along the interpolated path. Finally, the atomic positions of the interpolated structures are fully relaxed (while the basis vectors are fixed) which gives a 4 meV/fu barrier (the red dashed line in Fig. 3). Since the energy differences and barriers between end points are only few meV/fu, relatively low temperature could allow for fluctuations of Pnma-NPD $LiBH_4$ structure into the Pnma-SA structure. Thus, we suggests that the $LiBH_4$ potential energy surface is essentially flat, and it is easy to transfer from one $LiBH_4$ structure to another by keeping the Pnma space group with different lattice constants. We also notice that if fluctuations from Pnma-NPD to Pnma-SA occur with increasing temperature, the $\vec{a}$ lattice vector would increase, but $\vec{b}$ and $\vec{c}$ would decrease. Such thermal expansion indicates an anharmonicity in the $LiBH_4$ compound. This flat potential energy surface and anharmonicity phenomena agree well with the experimental thermal expansion observations[5]: with an increase in temperature from 90 K to 380 K, the Pnma unit cell volume increases by $\sim$2Å^3/fu, while the $\vec{b}$ vector initially expands upto 300 K but then continuously contracts on heating from 300 K to 380 K.

In conclusion, we have studied $LiBH_4$ in a variety of crystal structures using DFT free energy calculations. Our calculations show that the experimentally observed structure is the lowest energy in DFT. However, multiple $LiBH_4$ structures are degenerate with the experimental ground state crystal structure and there exists a relatively flat potential energy landscape between them. These degenerate structures include the recently theoretically predicted $LiBH_4$ structure[10], which the authors claimed to be $\sim$100 meV/fu lower in energy than the experimentally XRD determined $LiBH_4$ structure. Our calculations do not support these previous claims, and hence resolve this discrepancy between DFT and experiment. Moreover, it is interesting to notice that there is an energetic degeneracy of the ground state of other metal borohydrides, such as $Mg(BH_4)_2$ and $Ca(BH_4)_2$ although lattice constants and densities are

significantly different. In the $Mg(BH_4)_2$ compound, three crystal structures [space group: I4122 (a=7.448, b=7.448, c=12.15Å), F222 (a=12.122, b=10.362, c=10.741Å) and I-4m2 (a=8.165, b=8.165, c=10.126Å)] are degenerate in energy within 2 meV/fu[18]. In the $Ca(BH_4)_2$ compound, three $Ca(BH_4)_2$ structures [space group: Fddd (a=8.802, b=13.244, c=7.473Å), C2/c (a=7.51, b= 8.70, c=7.50Å, β=119.35), F2dd (a=8.77, b=13.02, c=7.41Å)] are degenerate in energy within 1 meV/fu[19]. This energetic degeneracy in metal borohydrides show evidence for the formation of different polymorphs depending on temperature and synthesis route[20–23].

The authors gratefully acknowledge financial support from the U.S. Department of Energy under Grant Nos. DE-FC36-08GO18136, DE-FG02-07ER46433, and funding from Ford Motor Company under the University Research Program.

---

[1] Y. Nakamori, K. Miwa, A. Ninomiya, H. Li, N. Ohba, S. Towata, A. Züttel, and S. Orimo, Phys. Rev. B **74**, 045126 (2006).
[2] L. Schlapbach and A. Züttel, Nature **414**, 353 (2001).
[3] J. Yang, A. Sudik, C. Wolverton, and D. J. Siegel, Chem. Soc. Rev. **39**, 656 (2010).
[4] N. Ohba, K. Miwa, M. Aoki, T. Noritake, S. Towata, Y. Nakamori, S. Orimo, and A. Züttel, Phys. Rev. B **74**, 075110 (2006).
[5] Y. Filinchuk, D. Chernyshov, and R. Cerny, J. Phys. Chem. C **112**, 10579 (2008).
[6] N. A. Zarkevich and D. D. Johnson, Phys. Rev. Lett. **100**, 040602 (2008).
[7] K. Miwa, N. Ohba, and S. Towata, Phys. Rev. B **69**, 245120 (2004).
[8] J. P. Soulié, G. Renaudin, R. Černý, and K. Yvon, J. Alloys Compd. **346**, 200 (2002).
[9] M. R. Hartman, J. J. Rush, T. J. Udovic, R. C. Bowman Jr., and S. J. Hwang, J. Solid State Chem. **180**, 1298 (2007).
[10] A. Tekin, R. Caputo, and A. Züettel, Phys. Rev. Lett. **104**, 215501 (2010).
[11] V. Ozolins, E. H. Majzoub, and C. Wolverton, J. Am. Chem. Soc. **131**, 230 (2008).
[12] G. Kresse and D. Joubert, Phys. Rev. B **59**, 1758 (1999).
[13] J. P. Perdew, K. Burke, and M. Ernzerhof, Phys. Rev. Lett. **77**, 3865 (1996).
[14] J. P. Perdew and Y. Wang, Phys. Rev. B **45**, 13244 (1992).
[15] P. Blaha, K.H. Schwarz, G.K. Madsen, D. Kvasnicka, and J. Luitz, **WIEN2k**, Techn. Universität Wien, Austria (2001). ISBN 3-9501031-1-2.
[16] H. J. Monkhorst and J. D. Pack, Phys. Rev. B **13**, 5188 (1976).
[17] C. Wolverton, V. Ozoliņš, and M. Asta, Phys. Rev. B **69**, 144109 (2004).
[18] X. Zhou, Q. Qian, J. Zhou, B. Xu, Y. Tian, and H. Wang, Phys. Rev. B **79**, 212102 (2009).
[19] E. H. Majzoub and E. Rönnebro, J. Phys. Chem. C **113**, 3352 (2009).
[20] C. Li, P. Peng, D. W. Zhou, and L. Wan, Int. J. Hydrogen Energy **36**, 14512 (2011).
[21] M. D. Riktor, M. H. Sørby, K. Chlopek, M. Fichtner, F. bouchter, A. Zuttel, B. C. Hauback, J. Mater. Chem. **17**, 4939 (2007).
[22] Y. filinchuk, E. Rönnebro, and D. Chandra, Acta Mater. **57**, 732 (2009).
[23] V. Ozolins, E. H. Majzoub, and C. Wolverton, Phys. Rev. Lett. **100**, 135501 (2008).